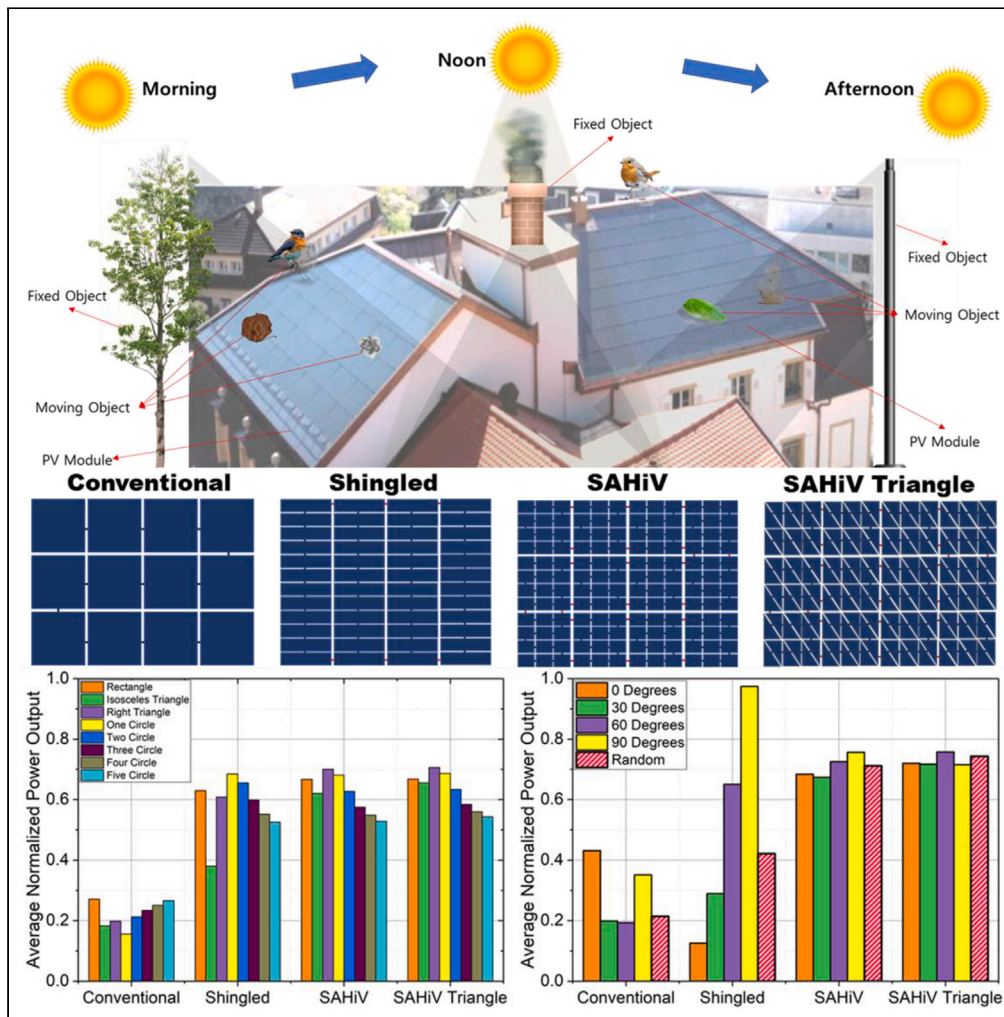


Article

# Small area high voltage photovoltaic module for high tolerance to partial shading



Luthfan Fauzan,  
Min Ju Yun, Yeon  
Hyang Sim, Dong  
Yoon Lee, Seung I.  
Cha

sicha@keri.re.kr

**Highlights**

SAHiV concept is pseudo-high-voltage low-current cells that can be connected in parallel

SAHiV outperforms conventional and shingled modules under partial shading condition

SAHiV modules are robust against all types of shading geometry and angles

SAHiV module is ideal for urban applications with unpredictable shadows and limited land



## Article

## Small area high voltage photovoltaic module for high tolerance to partial shading

Luthfan Fauzan,<sup>1,2</sup> Min Ju Yun,<sup>1</sup> Yeon Hyang Sim,<sup>1</sup> Dong Yoon Lee,<sup>1</sup> and Seung I. Cha<sup>1,2,3,\*</sup>

## SUMMARY

The urban application of photovoltaics is necessary to achieve carbon-free electricity production. However, the serial connections within modules cause problems under partial shading conditions, which is inevitable in urban applications. Therefore, a partial shading-tolerance photovoltaic module is needed. This research introduces the small-area-high-voltage (SAHiV) module with rectangle and triangle shapes for high partial shading tolerance and compares its performance with conventional and shingled modules. We tested it with discrete and continuous shading shape groups to represent unpredictable shading by simulations using LTspice with Monte Carlo simulation combined with latin hypercube sampling that were validated by comparison with experimental results. The SAHiV triangle module exhibited the best partial shading tolerance under most scenarios. Both types of SAHiV modules (rectangular and triangular) were robust against all types of shading patterns and angles, as indicated by their stable shading-tolerance values. These modules are thus suitable for use in urban areas.

## INTRODUCTION

Photovoltaics (PV) have the potential to become a major source of electricity.<sup>1,2</sup> The application of PV has penetrated deeply into urban life, and the PV potential in buildings has been estimated to meet one-third of the national electricity demand in most industrialized countries.<sup>3–6</sup> Building-applied photovoltaics (BAPVs) and building-integrated photovoltaics (BIPVs) will proliferate because of growing residential electricity costs and decreasing PV component costs.<sup>7</sup> BAPV and BIPV can save land use in urban areas, which are very limited and have high prices.<sup>6,8</sup> BIPV makes buildings become net zero consumption buildings and even a source of income because of current problems with PV, namely the cost component related to electricity transport.<sup>8,9</sup> However, data indicate that 70% of cars can run on solar energy, which makes vehicle-integrated photovoltaic (VIPV) systems extremely promising.<sup>10,11</sup> Thus, PV will play a critical role in energy decarbonization, especially in densely populated areas.<sup>1,6,12</sup>

A shortcoming of integrated PV, including BAPV, BIPV, and VIPV systems is that modules in urban settings can frequently or continuously all day long be subjected to shading caused by structures, such as buildings, poles, antennas, dormers, trees, birds, and even passing objects (dynamic shading).<sup>7,8,13–15</sup> Shading results in substantial power loss by string mismatch, which can reduce energy yield by 20–25%.<sup>11,16,17</sup> Shading causes a reverse-biased solar cell that changes power, known as a “hotspot”.<sup>18,19</sup> Hotspots cause a temperature increase in the cell to more than 100°C, which can damage the cell and cause a loss in output power of up to 25%.<sup>18–21</sup> Power loss due to shading occurs mainly in modules connected in series (strings); thus, the shading tolerance of a PV module can be increased by adding parallel interconnections (subgroups) or bypass diodes.<sup>13</sup> However, adding a parallel interconnection will reduce the voltage of the module.

Shingled modules are one of the proposed solutions to partial-shading power loss. Shingled modules have a better partial-shading tolerance than conventional modules.<sup>17,22</sup> However, in some cases, power losses in shingled modules can be greater than those in conventional modules.<sup>23</sup> Bae et al.,<sup>22</sup> Kunz et al.,<sup>23</sup> and Wen et al.<sup>24</sup> have shown that shingled modules exhibit excellent partial-shading tolerance in the horizontal shading pattern but poor tolerance in the vertical shading pattern. This characteristic of shingled modules will be a severe problem in urban applications. Klasen et al.<sup>25</sup> proposed a shingled matrix module with interconnection features and an additional lateral overlap of the solar cells. Matrix modules perform better than shingled modules but produce the same power in horizontal and vertical shading patterns.<sup>25,26</sup> Carr

<sup>1</sup>Energy Conversion Research Center, Electrical Materials Research Division, Korea Electrotechnology Research Institute, Changwon-si, Gyeongsangnam-do 51543, Korea

<sup>2</sup>Department of Electrofunctionality Materials Engineering, University of Science and Technology, Changwon-si, Gyeongsangnam-do 51543, Korea

<sup>3</sup>Lead contact

\*Correspondence: sicha@keri.re.kr

<https://doi.org/10.1016/j.isci.2023.106745>



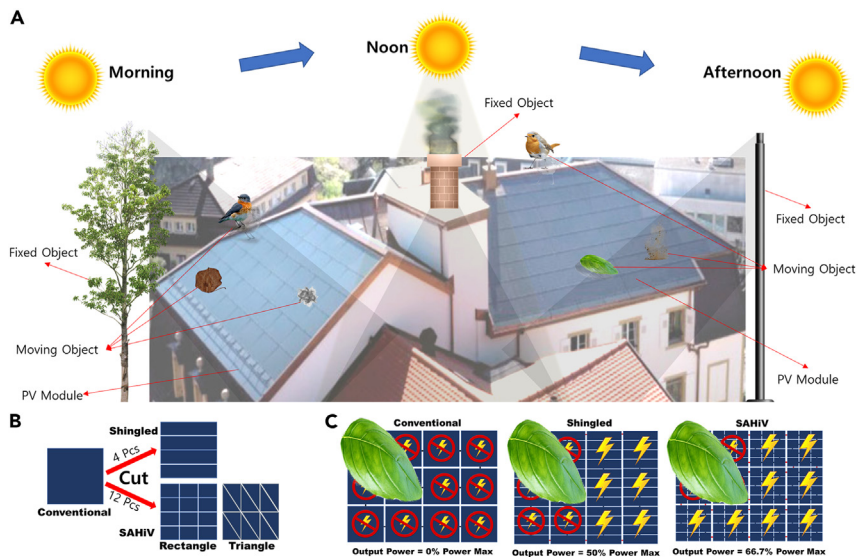


**Figure 1. Main concept of small-area-high-voltage-photovoltaic module**

(A) Shading scenarios in an urban environment. In urban scenarios, shading cannot be predicted because the shape of the shadow will always change following the sun's movement and because there are shadows of birds, leaves, and dust.

(B) Cell shape used in the present research. This research included four types of cells; conventional cells measuring 60 mm × 60 mm are divided horizontally into shingled cells (15 mm × 60 mm). The conventional cell is divided into 12 with a rectangular shape, resulting in the SAHIV cell (15 mm × 20 mm), and with a triangular shape, resulting in the SAHIV triangle cell (30 mm × 20 mm).

(C) Power output from conventional, shingled, and SAHIV modules under partial-shading conditions.

et al.<sup>27</sup> proposed using high-voltage modules, which divide cells into 16 units with one bypass diode to improve shade tolerance, known as "TESSERA." High-voltage modules can substantially increase annual energy yields under shading conditions.<sup>7,28</sup> Another benefit of high-voltage modules over conventional modules is that they use lower currents, which enables the use of smaller cables and bypass diodes, thereby lowering the cost of the materials.<sup>29</sup> Hanifi et al.<sup>30</sup> and Pannebakker et al.<sup>31</sup> proposed one diode per cell to prevent hotspots and increase the module's performance under shading conditions. Still, there is power dissipation in the diode and causing  $V_{MPP}$  to change. At the PV Array level, there is an approach to do PV Array configuration to handle partial shading, but it is challenging to apply for BAPV, BIPV, and VIPV, which only use a few modules.<sup>15,32</sup>

The concept of high-voltage cells is suggested in the present paper to improve shade tolerance. We propose a small-area-high-voltage (SAHIV) module as a pseudo-high-voltage module with rectangular and triangular shapes. The SAHIV that we propose is in rectangular and triangular shapes so that it can be applied according to the curvature of the area with flexible and stretchable solar cell technology.<sup>33,34</sup> We compare the shade-tolerance performance of a SAHIV with that of conventional and shingled modules in discrete and continuous shading groups. We test the shade-tolerance performance of the modules using Monte Carlo-based simulations and verification experiments with mini-modules. We analyze the magnitude of the power output module generated by the module from 32,500 randomly selected shading scenarios using latin hypercube sampling (LHS). Module performance under shading conditions is compared with the average normalized power for partial shading. We also carry out module analysis in shallow shadowing and heavy shadowing conditions. In addition, sensitivity to shading patterns scenarios is analyzed to determine the modules' performance in unpredictable situations.

## Small-area-high-voltage concept and simulation

### Small-area-high-voltage concept

In urban environments, the use of PV modules with high partial-shading tolerance is critical because of unpredictable shading conditions, as shown in Figure 1A. The partial-shading problem mainly occurs in strings-connected cells because the current generated will follow the lowest current of the cell in that

connection. It causes power loss and heat generation (i.e., a hotspot) that adversely affect the reliability and lifetime of the cells affected by the shadow. Cells connected in parallel exhibit superior partial-shading tolerance compared with cells connected in strings. Therefore, designing a module with a parallel connection is a fundamental solution to the partial-shading problem. However, the module voltage will be very low in a parallel connection. Designing a module with parallel connections of high-voltage and low-current cells is a basic solution but is impossible with commercial solar cells. Pseudo-high-voltage cells provide an alternative solution for modules with high partial-shading tolerance.

Small-area-high-voltage (SAHiV) is a concept we propose to fabricate pseudo-high-voltage low-current cells. SAHiV cells are prepared by cutting conventional cells into 12 pieces, as shown in [Figure 1B](#). We made SAHiV cells with two shapes: rectangular and triangular. We connected 12 cells in strings to become one subgroup to form a pseudo-high-voltage low-current cell with the same dimensions as a conventional cell. We also configured one subgroup of SAHiV cells as a group-like strings connection in conventional cells but with a parallel connection, making the resultant module more resistant to shadows. This design differs from that of shingled cells, where a module is divided into four to six pieces arranged in strings lengthwise and connected string subgroups to group with parallel connections to the side. The elongated shape of the shingled module causes the generated power to be strongly affected by the shape of the shadow. The difference compared to TESSERA is that we have an enlarged concept and give free shapes, size, and connection topology; whereas TESSERA is rectangular, including an integrated bypass diode. So SAHiV concept generalizes the idea to optimize the partial shading tolerance further. [Figure 1C](#) shows that the SAHiV module can produce more power than conventional and shingled modules, potentially making SAHiV modules suitable for use in urban areas.

### Simulation methods for partial shading on photovoltaics modules

In the present study, we employ the two-diode model<sup>35,36</sup> shown in [Equation 1](#) with ideality factors of the diode set to  $N_0 = 1$  and  $N_1 = 2$  (See [Figure S1](#)).

$$J(V) = J_{ph} - J_0 \left( \exp \left\{ \frac{q(V + JR_s)}{N_0 k_b T} \right\} - 1 \right) - J_1 \left( \exp \left\{ \frac{q(V + JR_s)}{N_1 k_b T} \right\} - 1 \right) - \frac{V + JR_s}{R_{sh}} \quad (\text{Equation 1})$$

where  $V$  is the terminal voltage,  $J_{ph}$  is the photogenerated current,  $J_0$  and  $J_1$  denote the saturation currents of the first (D1) and second (D2) diode, respectively,  $q = 1.6 \times 10^{-19}$  C is the electron charge,  $N_0$  and  $N_1$  denote the diode ideality factor of the first (D1) and second (D2) diode, respectively,  $k_b = 1.38 \times 10^{-23}$  J/K is Boltzmann's constant,  $T$  is the temperature,  $R_s$  is the series resistance, and  $R_{sh}$  is shunt resistance.

We simulated the output power results under shading situations using the LTspice circuit simulator. A SPICE simulation (simulation program with integrated circuit emphasis) was performed because it can rapidly simulate power output under any shade circumstances.<sup>25,37</sup> The parameter values were derived from the average measurement results for each solar cell size using the fitting method of Suckow et al.<sup>38,39</sup> (The detailed parameters are in [Table S1](#)).

We constructed modules with 12 cells connected in strings. The total active module area in all the modules was 432 cm<sup>2</sup>; the width and length of the modules were 240 and 180 mm, respectively. First, we constructed a conventional module with 12 string cells (cell size 60 mm × 60 mm with a square shape), as shown in [Figure 2A](#). In total, this module consisted of 12 conventional cells. Second, we constructed a shingled module with four subgroup cells, where each subgroup cell consisted of 12 string cells (cell size 15 mm × 60 mm with a rectangular shape), as shown in [Figure 2A](#). This module consisted of 48 shingled cells. Third, we constructed a SAHiV module with 12 subgroup cells, where each subgroup cell consisted of 12 string cells (cell size 15 mm × 20 mm with a rectangular shape), as shown in [Figure 2A](#). This module consisted of 144 SAHiV cells. Fourth, we fabricated a SAHiV triangle module with 12 subgroup cells, where each subgroup cell consisted of 12 string cells (cell size 30 mm × 20 mm with the right-triangle shape) as shown in [Figure 2A](#). This module consisted of 144 SAHiV triangle cells.

Shading tests were carried out with two groups of shading scenarios: eight discrete shading scenarios and five continuous shading scenarios. The discrete shading scenarios consisted of a rectangle, right triangle, isosceles triangle, one-circle, two-circle, three-circle, four-circle, and five-circle shapes (The detailed parameters are in [Tables S2–S9](#)). The continuous shading scenarios consisted of diagonal shading with angles

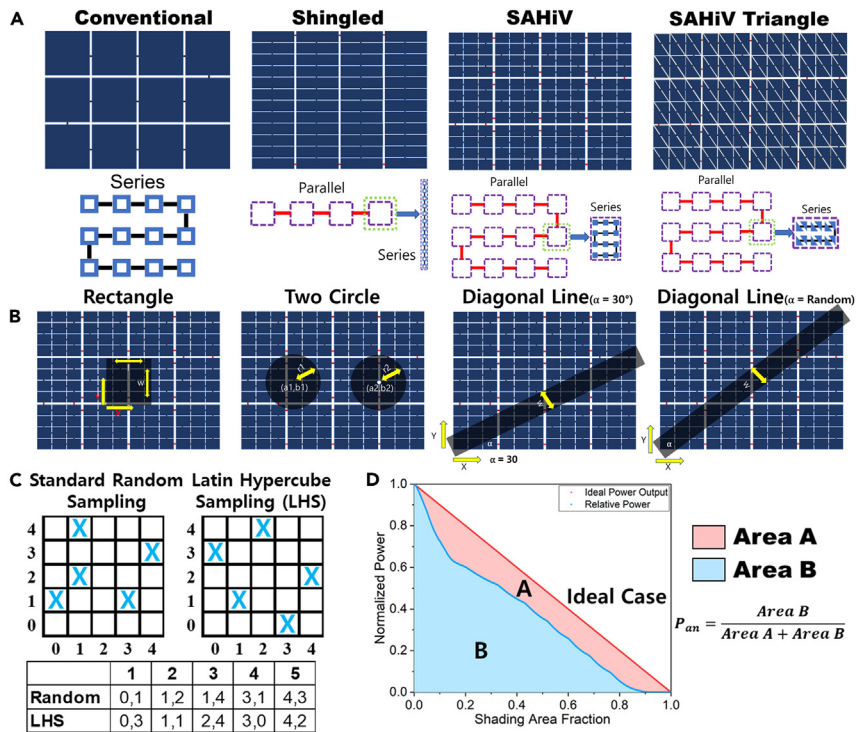


**Figure 2. Module layout and shading scenarios**

(A) Module layout used in the present research.

(B) The shading shape scenarios in the present research: a rectangle and two circles are used for discrete shading; a diagonal line with a 30° angle and a diagonal line with a random angle are used for continuous shading. (C) Difference between standard random sampling and Latin hypercube sampling (LHS). In LHS, numbers are chosen randomly by considering the multidimensional distribution.

(D) How  $P_{an}$  is calculated. The blue dot is the relative power generated under the shadow, and the red point is the power generated under ideal conditions.

of 0°, 30°, 60°, and 90° and a random angle. The shading parameter of shading was chosen by LHS. If shading was outside the layout module, we only measured the shading inside the module area. We limited the number of LHS parameter combinations to 2500. In total, we used more than 32,500 shading scenarios (see [Figures S2–S4](#) for details of the shading scenarios).

The discrete shading scenarios included several shapes of objects, including rectangles, triangles, and circles. In the case of circles, multiple shading objects were also simulated. Examples of discrete shading scenarios involving a rectangle and two circular shading shapes are shown in [Figure 2B](#) (for other discrete shading scenarios, see [Figure S2](#) and [S3](#)). The shading scenarios included the location and size of the shading (see [discrete shading scenarios parameter](#)).

In continuous shading scenarios, we varied the shading angle from 0° to 30°, 60°, and 90° or a random angle. This diagonal shading had three parameters: the starting coordinates of the diagonal shading ( $x$ ,  $y$ ) and the width of the diagonal shading ( $D_{width}$ ); parameters  $x$ ,  $y$ , and  $D_{width}$  ranged from 0 to 240, from 0 to 180, and from 0 to 300, respectively. Diagonal shading with a random angle had four parameters: the starting coordinates of the diagonal shading ( $x$ ,  $y$ ), the angle ( $\alpha$ ), and the width of the diagonal shading ( $D_{width}$ ). The values of  $x$ ,  $y$ , and  $D_{width}$  were fixed but  $\alpha$  varied from 0° to 90°. Diagonal shading with an angle of 30° and a random angle are shown in [Figure 2B](#), and parameters are in [Tables 1](#) and [2](#). Diagonal shading scenarios with angles of 0°, 60°, and 90° are shown in the [Supplemental information](#).

Under actual conditions, the shadow on a PV module cannot be predicted because of the unlimited number of scenarios. Consequently, we used Monte Carlo simulations in combination with LHS in the present work to select the scenarios randomly. LHS is a statistical technique for producing a multidimensional

**Table 1. Parameter limit for LHS of the diagonal shading scenarios with random angle**

Parameter	Lower limit	Upper limit
x (mm)	0	240
y (mm)	0	180
$\alpha$ (°/degree)	0	90
$D_{width}$ (mm)	0	300

distribution's parameter values in a random sample. LHS is frequently used to create computer experiments or Monte Carlo algorithms, which are computational algorithms that depend on repeated random sampling to produce numerical results.<sup>40</sup>

The shading parameters in the present study were randomly selected using the LHS method developed by Deutsch and Deutsch.<sup>41,42</sup> LHS was used to distribute the shading scenario selection across numerous scenarios. The difference between LHS and standard random sampling is shown in Figure 2C. In LHS, random value selection will consider the multidimensional distribution; thus, it is necessary to know the value of the previous sample and the number of samples. In a standard random sample, new sample points are created without considering the previous sample points.

We used the method of average normalized power for partial shading, as proposed by Klases et al.,<sup>17</sup> to evaluate the performance of the PV modules. We made adjustments by setting the irradiation of the shaded area to zero ( $I_{SO} = 0$ ) so that the lowest possible output was zero ( $P_{min} = 0$ ). The shading area fraction ( $A_{sh}$ ) in Figure 2D is the ratio between the shading area ( $A$ ) and the total PV module area ( $A_0$ ):

$$A_{sh} = \frac{A}{A_0} \quad \text{(Equation 2)}$$

$P_{ideal}$  is a condition when the power output produced is ideal according to the assumption that PV modules operate following irradiation equality.  $P_{ideal}$  is expressed by Equation 3:

$$P_{ideal} = P_{max}(1 - A_{sh}) \quad \text{(Equation 3)}$$

where  $P_{max}$  is the maximum power generated by the PV module when there is the shading fraction area is zero ( $A_{sh} = 0$ ).

The average normalized power for partial shading ( $P_{an}$ ) is described graphically in Figure 2D.  $P_{an}$  is calculated by measuring the area under  $P(A_{sh})$  divided by the area under  $P_{ideal}$ , where  $P(A_{sh})$  is the normalized power generated by the PV module when there is a shadow with area  $A_{sh}$ . The value of  $P_{an}$  is calculated using Equation 4, which is numerically worked out using the trapezoidal rule:

$$P_{an} = \frac{\int_0^1 P(A_{sh}) dA_{sh}}{\int_0^1 P_{ideal} dA_{sh}} = 2 \int_0^1 P(A_{sh}) dA_{sh} \quad \text{(Equation 4)}$$

### Validation of simulations by experiments

We validated our simulation method by comparing the simulation results with those of experiments. We compared the results of the four modules we tested in the present work. Four modules, whose sizes are shown in Figure 3A, were fabricated. Four cell sizes were used in the present study: 60 mm × 60 mm cells with a rectangular shape (conventional), 15 mm × 60 mm cells with a rectangular shape (shingled), 15 mm × 20 mm cells with a rectangular shape (SAHiV), and 30 mm × 20 mm cells with a right-triangle

**Table 2. Parameter limit for LHS of the diagonal line with angles of 0°, 30°, 60°, and 90° shading scenarios**

Parameter	Lower limit	Upper limit
x (mm)	0	240
y (mm)	0	180
$D_{width}$ (mm)	0	300

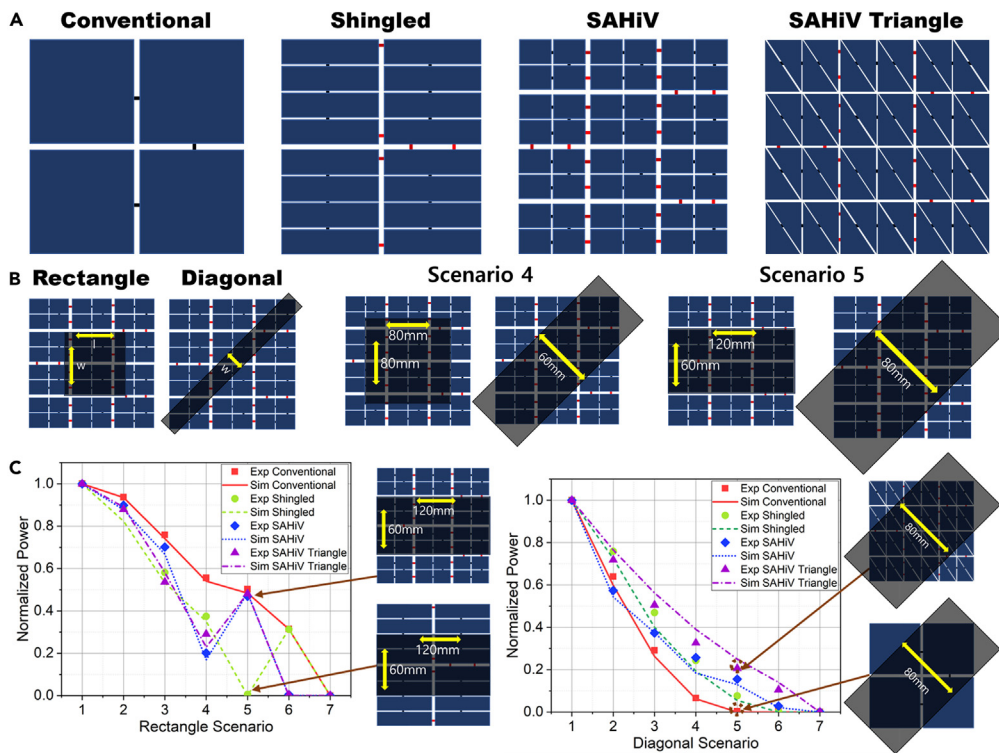


**Figure 3. Validation of simulation by experiments**

(A) Mini module layout used in the experiment to verify the simulation results.  
 (B) Example of shading scenarios used in the experiment. This scenario has rectangular and diagonal shading scenarios.  
 (C) Comparison of the experiment and simulation results. The left graph shows the results for the rectangle scenario, and the right graph shows the results for the diagonal scenario.

shape (SAHiV triangle). We fabricated all four of the modules to have active module areas of 144 cm<sup>2</sup>, with a width of 120 mm and a length of 120 mm, that shown in Figure S5.

We conducted shading experiments under 1 sun irradiation using an AM1.5 spectrum in a solar simulator. We conducted the experiments at 60°C module temperature to prevent power fluctuations due to temperature differences resulting from partial shading. We conducted measurements for each shading scenario three times and compared the average with the simulation results. The power compared is the normalized power.

We investigated seven discrete and continuous shading scenarios. For discrete shading scenarios, we chose a rectangular shape, as shown in Figure 2B; the length and width of the rectangular cells are shown in Table 3. For continuous shading scenarios, we chose a diagonal shape, as shown in Figure 3B; the width

**Table 3. Shading dimensions for experiment scenario of rectangle shading**

No	Length (mm)	Width (mm)
1	0	0
2	30	30
3	60	60
4	80	80
5	120	60
6	80	120
7	120	120

**Table 4. Shading dimensions for experiment scenario of diagonal shading**

No	Width (mm)
1	0
2	20
3	40
4	60
5	80
6	100
7	170 (all)

of the diagonal cells is shown in Table 4. In scenario 4, the rectangle shading has a length of 80 mm and width of 80 mm, and the diagonal shading has a width of 60 mm, as shown in Figure 3B. In scenario 5, the rectangle shading has a length of 120 mm and a width of 60 mm, and the diagonal shading has a width of 80 mm, as shown in Figure 3B.

The results of the experiments and simulations are shown in Figure 3C. The left graph shows the results of the rectangle shading scenarios, and the right graph shows the results of the diagonal shading scenarios. In both scenarios, the simulation and experiment results are well matched, with a maximum error of 0.07. (*I-V* Curve Comparison between Experiment and Simulation is shown in Figure S6).

## RESULTS AND DISCUSSION

### Robustness of simulation

We investigated the robustness of the average normalized power for partial shading ( $P_{an}$ ) using four sets of shading patterns ranging from 10 to 2500 scenarios per data point. This aims to find out whether the simulation is robust or not. Scenario selection is made using LHS independently by simulating several different scenarios. We perform two tests to represent each group of scenarios. Discrete scenarios consist of a rectangle and two-circle shading. Continuous scenarios consist of diagonal shading with a random angle and diagonal shading with an angle of 30°, as shown in Figure 4A.

In the discrete shading scenarios, our simulation shows that the results are stable when the number of scenarios is 150–200. When more than 200 rectangle shading scenarios are used, we observe  $P_{an} = 0.263 \pm 0.007$  for the conventional layout,  $P_{an} = 0.629 \pm 0.005$  for the shingled layout,  $P_{an} = 0.664 \pm 0.009$  for the SAHiV layout, and  $P_{an} = 0.666 \pm 0.008$  for the SAHiV triangle layout. In the two-circle shading, we observe  $P_{an} = 0.213 \pm 0.006$  for the conventional layout,  $P_{an} = 0.652 \pm 0.007$  for the shingled layout,  $P_{an} = 0.620 \pm 0.007$  for the SAHiV layout, and  $P_{an} = 0.627 \pm 0.007$  for the SAHiV triangle layout. The “errors” for the selected data points refer to the standard deviations of the  $P_{an}$  values. On the basis of the trajectory of the plotted data and the small errors, we deduced that  $P_{an}$  is a robust value when the number of scenarios is greater than 200.

In the continuous shading scenarios, our simulation results are stable when the number of scenarios is 400–500. The  $P_{an}$  values larger than 500 in diagonal shading with a random angle, we observe  $P_{an} = 0.214 \pm 0.004$  for the conventional layout,  $P_{an} = 0.415 \pm 0.012$  for the shingled layout,  $P_{an} = 0.712 \pm 0.003$  for the SAHiV layout, and  $P_{an} = 0.744 \pm 0.002$  for the SAHiV triangle layout. In the diagonal shading with an angle of 30°, we observe  $P_{an} = 0.196 \pm 0.004$  for the conventional layout,  $P_{an} = 0.289 \pm 0.002$  for the shingled layout,  $P_{an} = 0.674 \pm 0.001$  for the SAHiV layout, and  $P_{an} = 0.718 \pm 0.001$  for the SAHiV triangle layout. We observe that  $P_{an}$  exhibits robust values for a small number of scenarios compared with considering infinite scenarios for all shading scenarios. Robustness value checking is carried out to prove that the sampling method used to obtain  $P_{an}$  (expected value) can show the actual average normalized power value for partial shading. On the basis of the simulation results, we conclude that our simulation can be used to test the behavior of partial shadows for the four module layouts.

### Area graph of shading

We used an area graph of shading to determine the modules’ performance against various shapes and sizes of shadows. Figure 4B shows the area graphs of shading for the rectangle shading, two-circle shading,

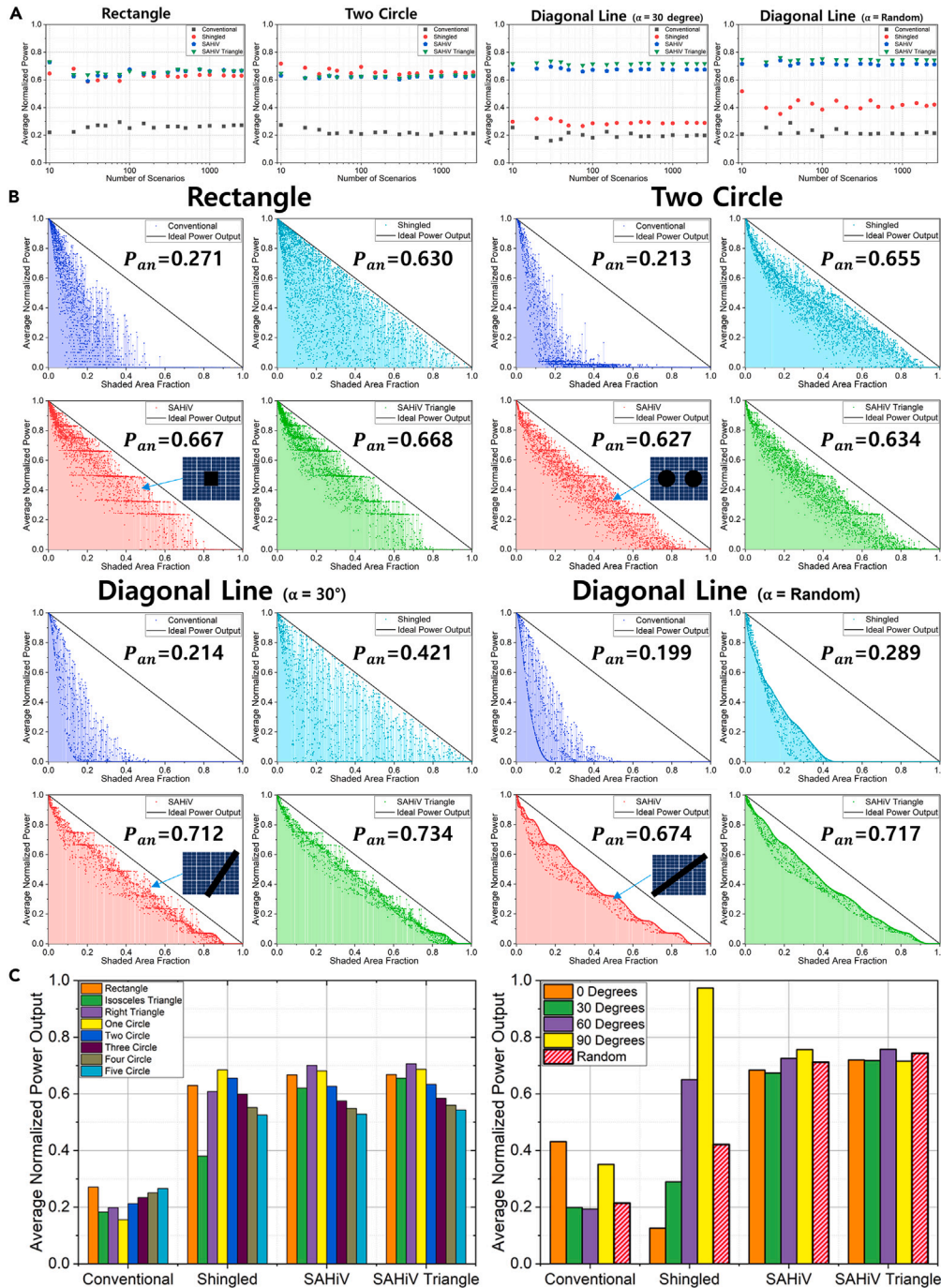


**Figure 4. Robustness and results of simulation**

(A) Robustness of the system. Testing is done by performing simulations ranging from 10 to 2500 scenarios.

(B) Area graphs of shading with a rectangle, two circles, a diagonal line with a  $30^\circ$  angle, and a diagonal line with a random angle. Purple, blue, red, and green graphs represent the results for the conventional module, shingled module, SAHIV module, and SAHIV triangle module, respectively. Each point in the graph represents one shading scenario.

(C) Graph of the  $P_{an}$  values. The left graph shows the results for the discrete shading group, and the right graph shows the results for the continuous shading group.

diagonal shading with an angle of  $30^\circ$ , and random-angle-of-shading scenario and the four module layouts according to the legend of each layer (Another area graph of shading is shown in [Figures S7–S9](#)). Each data point corresponds to a particular scenario. We chose 2500 points instead of 200 when the result was already robust because we could observe the distribution of scenarios and understand the module layout's features more clearly.

In [Figure 4B](#), the conventional modules have  $P_{an} = 0.271$  for rectangle shading,  $P_{an} = 0.213$  for two-circle shading,  $P_{an} = 0.199$  for diagonal shading with an angle of  $30^\circ$ , and  $P_{an} = 0.214$  for diagonal shading with a random angle. The point distribution of the conventional module shown in the graph has the same features. The conventional module only produces power when the shading fraction area is less than 0.2–0.3; at larger shading fraction areas, the module produces little power. This means the conventional modules can only produce power when encountering a small shadow area. So, the conventional module is not suitable for areas with partial shading. This phenomenon occurs under all the investigated shading scenarios in [Figures 4B](#) and [S7–S9](#).

Shingled modules have  $P_{an} = 0.630$  for rectangle shading,  $P_{an} = 0.655$  for two-circle shading,  $P_{an} = 0.289$  for diagonal shading with an angle of  $30^\circ$ , and  $P_{an} = 0.421$  for diagonal shading with a random angle. The point distribution of the shingled module as shown in the graph exhibits different features among other modules. The point distribution for the shingle module shows good features for the two-circle scenarios; however, in diagonal shading with an angle of  $30^\circ$ , the features are similar to those of the conventional module. In rectangle shading and diagonal shading with an angle of  $30^\circ$ , the point distribution is spread. When the shading fraction area is 0.08, the normalized power produced is in the range of 0.00042–0.87622. Another graph in [Figures S7–S9](#) shows that the point distribution for the shingled module depends on the shading shape. This means that the shingled module cannot be used with all types of shadow scenarios. So that shingled modules are less suitable for urban areas that have shading in various forms.

The SAHiV modules have  $P_{an} = 0.667$  for rectangle shading,  $P_{an} = 0.627$  for two-circle shading,  $P_{an} = 0.674$  for diagonal shading with an angle of  $30^\circ$ , and  $P_{an} = 0.712$  for diagonal shading with a random angle. The SAHiV triangle modules have  $P_{an} = 0.668$  for rectangle shading,  $P_{an} = 0.634$  for two-circle shading,  $P_{an} = 0.717$  for diagonal shading with an angle of  $30^\circ$ , and  $P_{an} = 0.734$  for diagonal shading with a random angle. The point distributions of the SAHiV and SAHiV triangle modules as shown in the graph exhibit the same features. Both modules exhibit good shading features in all the scenarios; however, the SAHiV triangle module shows slightly better results than the SAHiV module. This shows that the SAHiV module suits urban areas with unpredictable shadows. This phenomenon occurs in all the shading scenarios represented in [Figures 4B](#) and [S7–S9](#).

### Average normalized power for partial shading ( $P_{an}$ ) result by module layout

We compare the  $P_{an}$  values to find the average normalized power output of modules under partial shading.  $P_{an}$  values are a statistical method used to evaluate module performance in dealing with partial shading. The graph in [Figure 4C](#) shows the shading tolerance of the modules and the  $P_{an}$  values. The graph shows that, in most of the shading scenarios, the SAHiV triangle demonstrates the best partial shading tolerance, with a  $P_{an}$  that does not substantially change. In the case of two-circle shading, three-circle shading, and diagonal shading with an angle of  $90^\circ$ , the shingled module demonstrates the best partial shading tolerance. However, among the investigated modules, the shingled module demonstrates the worst shading performance under diagonal shading with an angle of  $0^\circ$ .

The  $P_{an}$  results indicate that the conventional module demonstrates the worst performance under most scenarios. The  $P_{an}$  values for the conventional module range from 0.156 to 0.271 for discrete shading and from 0.193 to 0.431 for continuous shading. For the shingled module, the  $P_{an}$  results are unstable, ranging from 0.380 to 0.685 for discrete shading and from 0.126 to 0.974 for continuous shading. The shingled module performs well in certain scenarios but is highly sensitive to the shading shape and angle. This effect is evident in [Figure 4C](#) for shingled modules with very different values.

In the case of the SAHiV module, the  $P_{an}$  shows good results, ranging from 0.529 to 0.701 for discrete shading and from 0.674 to 0.756 for continuous shading. Likewise, the  $P_{an}$  shows good results for the SAHiV

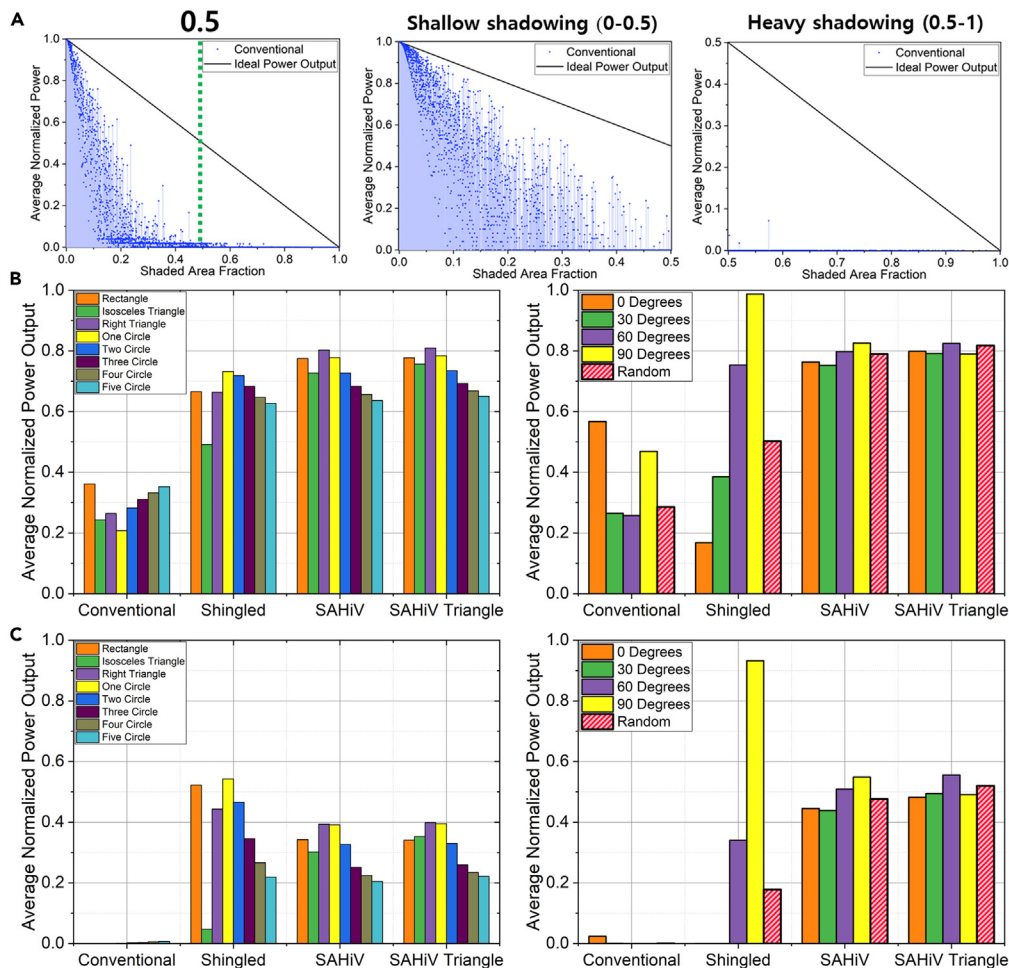


**Figure 5. Results for shallow shadowing and heavy shadowing**

(A) The differences in shading scenarios of shallow shadowing (0–50%) and heavy shadowing (50–100%).

(B) Results corresponding to shallow shadowing (0–50%). The left graph shows the results for the discrete shading group, and the right graph shows the results for the continuous shading group.

(C) Results corresponding to heavy shadowing (50–100%). The left graph shows the results for the discrete shading group, and the right graph shows the results for the continuous shading group.

triangle module, ranging from 0.543 to 0.707 for discrete shading and from 0.715 to 0.758 for continuous shading. These results indicate that both the SAHiV and SAHiV triangle modules are less sensitive to the partial shading geometry. Both modules have  $P_{an}$  values in the range of 0.529–0.758; however, the SAHiV triangle module exhibits better partial shading tolerance. SAHiV triangle performs slightly better than the SAHiV rectangle, but in actual practice choosing SAHiV rectangle or triangle can be adjusted according to the application’s needs.

When considering the distribution of each shading scenario in the area graph of shading, we find that the shading areas with shallow shadowing (0–50%) and heavy shadowing (50–100%) lead to a different phenomenon for each module. Figure 5A shows that if we divide the graph into shallow shadowing (0–50%) and heavy shadowing (50–100%) regions, the shading scenarios have different data point distributions. We calculate  $P_{an}$  for shallow and heavy shading to compare modules’ performance under both conditions more clearly. The method used to calculate  $P_{an}$  is the same as when calculating the 0–100% shading area with adjustment of the shading area divided into shallow shadowing (0–50%) and heavy shadowing (50–100%):

$$P_{an, \text{shallow shading}} = P_{an1} = \frac{\int_0^{0.5} P(A_{sh}) dA_{sh}}{\int_0^{0.5} P_{ideal} dA_{sh}} = \frac{8}{3} \int_0^{0.5} P(A_{sh}) dA_{sh} \quad (\text{Equation 5})$$

$$P_{an, \text{heavy shading}} = P_{an2} = \frac{\int_{0.5}^1 P(A_{sh}) dA_{sh}}{\int_{0.5}^1 P_{ideal} dA_{sh}} = 8 \int_{0.5}^1 P(A_{sh}) dA_{sh} \quad (\text{Equation 6})$$

For the conventional module under shallow shading (0–50%),  $P_{an1}$  ranges from 0.208 to 0.362 for discrete shading and from 0.257 to 0.567 for continuous shading. For the shingled module under shallow shading (0–50%),  $P_{an1}$  ranges from 0.491 to 0.732 for discrete shading and from 0.168 to 0.988 for continuous shading. For the SAHiV module under shallow shading (0–50%),  $P_{an1}$  ranges from 0.636 to 0.803 for discrete shading and from 0.752 to 0.826 for continuous shading. For the SAHiV triangle module under shallow shading (0–50%),  $P_{an1}$  ranges from 0.650 to 0.809 for discrete shading and from 0.790 to 0.825 for continuous shading. Thus, the SAHiV and SAHiV triangle modules show good partial shading tolerance under shallow shading (0–50%). The SAHiV and SAHiV triangle modules also show relatively stable values in all scenarios compared to other modules.

For the conventional module under heavy shading (50–100%),  $P_{an2}$  ranges from 0.000 to 0.007 for discrete shading and from 0.000 to 0.024 for continuous shading. For the shingled module under heavy shading (50–100%),  $P_{an2}$  ranges from 0.047 to 0.543 for discrete shading and from 0.000 to 0.932 for continuous shading. For the SAHiV module under heavy shading (50–100%),  $P_{an2}$  ranges from 0.204 to 0.393 for discrete shading and from 0.439 to 0.549 for continuous shading. For the SAHiV triangle module under heavy shading (50–100%),  $P_{an2}$  ranges from 0.221 to 0.398 for discrete shading and from 0.482 to 0.556 for continuous shading. Thus, conventional modules produce almost zero power under all of the shading scenarios involving heavy shading (50–100%), whereas the shingled module exhibits good partial shading tolerance compared with other modules under discrete shading scenarios involving heavy shading (50–100%). But the shingled module shows awful results for isosceles triangle shapes. In the continuous shading scenarios, the SAHiV and SAHiV triangle module offers the best and most stable results than other modules. The SAHiV and SAHiV triangle modules generally show the best results for shallow and heavy shading.

### Sensitivity to shading patterns scenarios

The distribution of shading scenarios exhibits a pattern in the area of the shading graph. We found that the distribution of points on the shaded-area graph shows a different pattern among the modules with different layouts. Figure 6A shows the patterns under different shading scenarios. Figure 6A is the graph for the shingled module. The graph has a vertical pattern, which means that, with the same shaded area, the power output of the module fluctuates widely. The right side of Figure 6A shows a shading area fraction ( $A_{sh}$ ) of  $\sim 0.11$ . The normalized power varies from 0.0004 to 0.8799. This means that when the shingled module is exposed to a shadow of about 11% of the module area, the power module production can vary from 0.04% to 87.99% of the module's maximum power. These phenomena occur for the continuous shading shown in Figure 6B and for the discrete shading shown in Figure S11. Thus, the shingled module is highly sensitive to the shading angle and shape, which poses a massive problem in real situations because we cannot predict shading shapes. In the case of the conventional module shown in Figure 5A, the distribution of points on the shaded-area graph is similar to the shingled module with a vertical pattern. The difference between conventional and shingled modules is that in conventional modules, after shading area fraction ( $A_{sh}$ ) of more than 0.3, the power output is almost 0.

Figure 6B shows the graph for the SAHiV module. The graph exhibits a horizontal pattern, which means the module produces similar power when the shading area does not substantially change. The right side of Figure 6B shows that the normalized power is  $\sim 0.74$  when the shading area fraction ( $A_{sh}$ ) ranges from 0.10 to 0.20. This means the SAHiV module will generate around 74% of the maximum power when covered in shadows of 10%–20% of the module area. This phenomenon occurs in both continuous shading (Figure 6B) and discrete shading (Figure S11). These results indicate that SAHiV modules are robust against changes in the shading shape as long as the shading area does not dramatically change. This module feature is beneficial in real situations because shading shapes cannot be predicted.

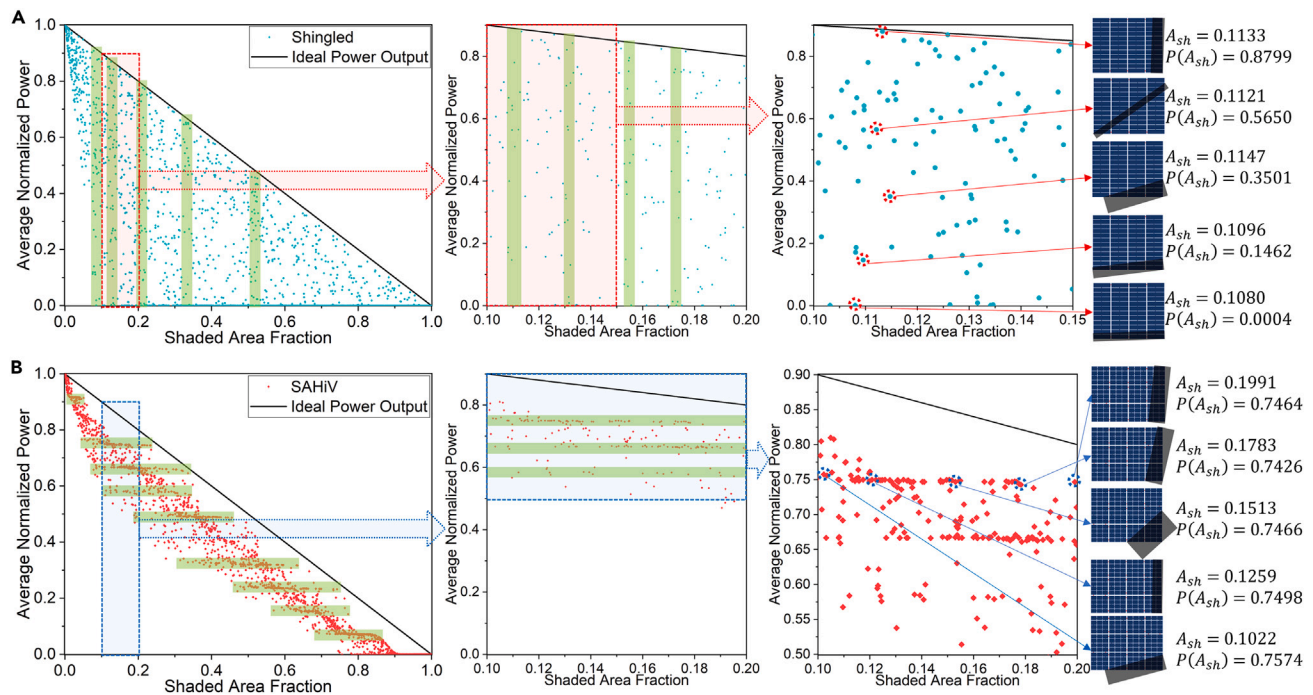


**Figure 6. Power shading pattern in diagonal shading shade**

(A) Power shading pattern in the shingled module. The shingled module has horizontal patterns for which the shading shape and normalized power are shown on the right side.

(B) Power shading pattern in the SAHiV module. The SAHiV module has a vertical pattern for which the shading shape and normalized power are shown on the right side.

## Conclusion

Our results show that SAHiV is a meaningful approach for partial shading problems. Both SAHiV and SAHiV triangle modules are less sensitive to the partial-shading geometry. Conversely, a shingled module performs well in some scenarios but is very sensitive to the shading shape and angle. In the conventional module case, the module is sensitive to various shading scenarios. We found that the SAHiV triangle module demonstrates better partial shading tolerance under most of the investigated scenarios.

We also found that shallow shadowing (0–50%) and heavy shadowing (50–100%) of the shading areas result in different module behaviors. Under shallow shadowing (0–50%), the SAHiV and SAHiV triangle modules exhibit good partial shading tolerance. Under heavy shadowing (50–100%), the shingled module exhibits good partial shading tolerance compared with the other modules under discrete shading scenarios, whereas conventional modules produce almost zero power under all of the shading scenarios.

We further found that the modules are sensitive to the shading pattern. For the shingled module shown in the horizontal shading pattern, the shading area power of the module fluctuates dramatically. This pattern means that the shingled module is highly sensitive to shading shapes, which is problematic in real situations because we cannot predict shading shapes. For the SAHiV and SAHiV triangle modules in the vertical shading pattern, slight changes in the total shading area result in the same power. The SAHiV modules are robust against changes in the shading shape as long as the shading area is similar. The results of this study indicate that the SAHiV module is very suitable for urban applications with unpredictable shadows and limited land. Under these conditions, the SAHiV module will increase its performance by 1.5–3 times compared to conventional modules, maximizing electricity production. The adjustable SAHiV concept fits perfectly with BAPV, BIPV, and VIPV as electricity costs continue rising and PV component prices continue declining. In addition, electricity can be used directly without enormous electricity transmission costs. Our future work will focus on full-scale modules with a diode to elucidate the optimum cell size.

### Limitations of the study

This study uses mini-sized photovoltaic modules in simulations and experiments and does not include diodes which make it different from commercially available photovoltaic modules. This simulation is also carried out under ideal conditions that do not consider temperature changes, gaps between cells, and other losses. The light conditions in this experiment are only no light (0 sun) or 1 sun condition, so there are no light conditions, such as when sunlight is blocked by clouds, trees, and so on. The simulated shading scenarios are also very limited to the two-dimensional shapes, with only 2500 scenarios for each shape compared to the unlimited number of shapes and forms of shading scenarios in the real application.

### Discrete shading scenarios parameter

Rectangle shading has four parameters: start point of the rectangle shading ( $x, y$ ), length, and width.  $x$  has a parameter range from 0 to 240, and  $y$  has a parameter range from 0 to 180. Length and width are determined size of the shading, length has a parameter range from 0 to 240, and width has a parameter range from 0 to 180. Figure 2B shows the shape of the rectangle shading shape and the parameter in Table S2.

Right-triangle shading has three parameters: start point of the right-triangle shading ( $x, y$ ), and length.  $x$  has a parameter range from 0 to 240, and  $y$  has a parameter range from 0 to 180. Length is determined size of the shading with a parameter range from 0 to 420. Figure S2A shows the shape of the right-triangle shading and the parameter in Table S3.

Isosceles triangle shading has three parameters: start point of the isosceles triangle shading ( $x, y$ ), and height.  $x$  has a parameter range from 0 to 240, and  $y$  has a parameter range from  $-120$  to 180. Height is determined size of the shading with a parameter range from 0 to 240. Figure S2B shows the shape of the isosceles triangle shading and the parameter in Table S4.

One-circle shading has three parameters: the center point of the circle shading ( $a_1, b_1$ ), and radius ( $r_1$ ).  $a_1$  has a parameter range from 0 to 240, and  $b_1$  has a parameter range from 0 to 180.  $r_1$  is the circle's radius with a parameter range from 0 to 160. Figure S3A shows one-circle shading shape, and the parameter is in Table S5.

Two-circle shading has six parameters: the center point of the first circle shading ( $a_1, b_1$ ), radius of first circle ( $r_1$ ), the center point of the second circle shading ( $a_2, b_2$ ), and radius of second circle ( $r_2$ ).  $a_1$  and  $a_2$  have a parameter range from 0 to 240.  $b_1$  and  $b_2$  have a parameter range from 0 to 180.  $r_1$  and  $r_2$  are the circle radii with a parameter range from 0 to 120. Figure 2B shows two-circle shading shapes and the parameter in Table S6.

We do other multiple-circle shadings that are three, four, and five-circle shading. Three-circle shading has nine parameters:  $a_1, b_1, r_1, a_2, b_2, r_2, a_3, b_3,$  and  $r_3$ . Four-circle shading has 12 parameters:  $a_1, b_1, r_1, a_2, b_2, r_2, a_3, b_3, r_3, a_4, b_4,$  and  $r_4$ . Five-circle shading has 15 parameters:  $a_1, b_1, r_1, a_2, b_2, r_2, a_3, b_3, r_3, a_4, b_4, r_4, a_5, b_5,$  and  $r_5$ . The parameters are set similarly to two-circle shading scenarios but with different radius parameters. Three-circle shading uses 0 to 100 for the radius parameter, four-circle shading use 0 to 90 for the radius parameter, and five-circle shading use 0 to 80 for the radius parameter. Figures S3B–S3D show shading shape, and Tables S7–S9 shows parameter for three, four, and five-circle shading scenarios, respectively.

### STAR★METHODS

Detailed methods are provided in the online version of this paper and include the following:

- KEY RESOURCES TABLE
- RESOURCE AVAILABILITY
  - Lead contact
  - Materials availability
  - Data and code availability
- EXPERIMENTAL MODEL AND SUBJECT DETAILS

### SUPPLEMENTAL INFORMATION

Supplemental information can be found online at <https://doi.org/10.1016/j.isci.2023.106745>.

## ACKNOWLEDGMENTS

This research was supported by the Korea Electrotechnology Research Institute (KERI), South Korea Primary Research Program through the National Research Council of Science & Technology (NST), South Korea, funded by the Ministry of Science and ICT (MSIT), South Korea (No. 23A01010).

## AUTHOR CONTRIBUTIONS

L.F. and S.I.C. suggested a new SAHiV PV module concept, conducted simulation and experimental details and wrote the draft manuscript, and reviewed it.

M.J.Y. and Y. H. S. contributed to detailed experiments for fabrication, measurement, and investigation.

D. Y. L. contributed to analyzing the shading tolerance response of the SAHiV PV module.

All authors have reviewed the manuscript and agreed regarding its submission.

## DECLARATION OF INTERESTS

The authors declare no competing interests.

Received: December 14, 2022

Revised: April 4, 2023

Accepted: April 21, 2023

Published: April 25, 2023

## REFERENCES

- Ballif, C. (2020). Introduction. In *Solar Cells and Modules*, A. Shah, ed. (Springer International Publishing), pp. 1–15. [https://doi.org/10.1007/978-3-030-46487-5\\_1](https://doi.org/10.1007/978-3-030-46487-5_1).
- Lesk, C., Csala, D., Hasse, R., Sgouridis, S., Levesque, A., Mach, K.J., Horen Greenford, D., Matthews, H.D., and Horton, R.M. (2022). Mitigation and adaptation emissions embedded in the broader climate transition. *Proc. Natl. Acad. Sci. USA* 119, e2123486119. <https://doi.org/10.1073/pnas.2123486119>.
- Peng, C., Huang, Y., and Wu, Z. (2011). Building-integrated photovoltaics (BIPV) in architectural design in China. *Energy Build.* 43, 3592–3598. <https://doi.org/10.1016/j.enbuild.2011.09.032>.
- Santos, Í.P.d., and Rüter, R. (2012). The potential of building-integrated (BIPV) and building-applied photovoltaics (BAPV) in single-family, urban residences at low latitudes in Brazil. *Energy Build.* 50, 290–297. <https://doi.org/10.1016/j.enbuild.2012.03.052>.
- Shukla, A.K., Sudhakar, K., Baredar, P., and Mamat, R. (2018). Solar PV and BIPV system: barrier, challenges and policy recommendation in India. *Renew. Sustain. Energy Rev.* 82, 3314–3322. <https://doi.org/10.1016/j.rser.2017.10.013>.
- Virtuani, A. (2020). Solar photovoltaics on land, water, and buildings. In *Solar Cells and Modules*, A. Shah, ed. (Springer International Publishing), pp. 285–306. [https://doi.org/10.1007/978-3-030-46487-5\\_11](https://doi.org/10.1007/978-3-030-46487-5_11).
- Sinapis, K., Rooijackers, T., Slooff, L., Okel, L., Jansen, M., and Carr, A. (2017). Towards new module and system concepts for linear shading response. In 2017 IEEE 44th Photovoltaic Specialist Conference (PVSC), pp. 1081–1085. <https://doi.org/10.1109/PVSC.2017.8366744>.
- Fairbrother, A., Quest, H., Özkalay, E., Wälchli, P., Friesen, G., Ballif, C., and Virtuani, A. (2022). Long-term performance and shade detection in building integrated photovoltaic systems. *Solar RRL* 6, 2100583. <https://doi.org/10.1002/solr.202100583>.
- Gholami, H., and Røstvik, H.N. (2020). Economic analysis of BIPV systems as a building envelope material for building skins in Europe. *Energy* 204, 117931. <https://doi.org/10.1016/j.energy.2020.117931>.
- Masuda, T., Araki, K., Okumura, K., Urabe, S., Kudo, Y., Kimura, K., Nakado, T., Sato, A., and Yamaguchi, M. (2017). Static concentrator photovoltaics for automotive applications. *Sol. Energy* 146, 523–531. <https://doi.org/10.1016/j.solener.2017.03.028>.
- Araki, K., Ji, L., Kelly, G., Agudo, E., Anton, I., Baudrit, M., Carr, A., Herrero, R., Kurtz, S., Liu, Z., et al. (2019). Modeling and standardization researches and discussions of the car-roof PV through international web meetings. In 2019 IEEE 46th Photovoltaic Specialists Conference (PVSC), pp. 2722–2729. <https://doi.org/10.1109/PVSC40753.2019.8980555>.
- Nowak, S. (2020). Photovoltaics in the future energy system. In *Solar Cells and Modules*, A. Shah, ed. (Springer International Publishing), pp. 321–339. [https://doi.org/10.1007/978-3-030-46487-5\\_13](https://doi.org/10.1007/978-3-030-46487-5_13).
- Calcabrini, A., Weegink, R., Manganiello, P., Zeman, M., and Isabella, O. (2021). Simulation study of the electrical yield of various PV module topologies in partially shaded urban scenarios. *Sol. Energy* 225, 726–733. <https://doi.org/10.1016/j.solener.2021.07.061>.
- Götz, D., Hahn, D., Gottschalg, R., Daßler, D., Schindler, S., and Hanifi, H. (2019). Evaluation of shading tolerance of PV modules with different module designs for mobile application by simulation, indoor and outdoor measurements. In 36th European Photovoltaic Solar Energy Conference and Exhibition, pp. 1504–1508. <https://doi.org/10.4229/EUPVSEC20192019-5CV.3.43>.
- Pachauri, R.K., Mahela, O.P., Sharma, A., Bai, J., Chauhan, Y.K., Khan, B., and Alhelou, H.H. (2020). Impact of partial shading on various PV Array configurations and different modeling approaches: a comprehensive review. *IEEE Access* 8, 181375–181403. <https://doi.org/10.1109/ACCESS.2020.3028473>.
- Al-Janahi, S.A., Ellabban, O., and Al-Ghamdi, S.G. (2020). A novel BIPV reconfiguration algorithm for maximum power generation under partial shading. *Energies* 13, 4470. <https://doi.org/10.3390/en13174470>.
- Klasen, N., Lux, F., Weber, J., Roessler, T., and Kraft, A. (2022). A comprehensive study of module layouts for silicon solar cells under partial shading. *IEEE J. Photovolt.* 12, 546–556. <https://doi.org/10.1109/JPHOTOV.2022.3144635>.
- Feng, X., and Ma, T. (2023). Solar photovoltaic system under partial shading and perspectives on maximum utilization of the shaded land. *Int. J. Green Energy* 20, 378–389. <https://doi.org/10.1080/15435075.2022.2047977>.

19. Ziar, H., Asaei, B., Farhangi, S., Korevaar, M., Isabella, O., and Zeman, M. (2017). Quantification of shading tolerability for photovoltaic modules. *IEEE J. Photovolt.* 7, 1390–1399. <https://doi.org/10.1109/JPHOTOV.2017.2711429>.
20. Dhimish, M., and Lazaridis, P.I. (2021). An empirical investigation on the correlation between solar cell cracks and hotspots. *Sci. Rep.* 11, 23961. <https://doi.org/10.1038/s41598-021-03498-z>.
21. Guerriero, P., Napoli, F. di, Coppola, M., and Daliento, S. (2016). A new bypass circuit for hot spot mitigation. In 2016 International Symposium on Power Electronics, Electrical Drives, Automation and Motion (SPEEDAM), pp. 1067–1072. <https://doi.org/10.1109/SPEEDAM.2016.7525991>.
22. Bae, J., Jee, H., Park, Y., and Lee, J. (2021). Simulation-based shading loss analysis of a shingled string for high-density photovoltaic modules. *Appl. Sci.* 11, 11257. <https://doi.org/10.3390/app112311257>.
23. Kunz, O., Evans, R.J., Juhl, M.K., and Trupke, T. (2020). Understanding partial shading effects in shingled PV modules. *Sol. Energy* 202, 420–428. <https://doi.org/10.1016/j.solener.2020.03.032>.
24. Wen, Z., Chen, J., Cheng, X., Niu, H., and Luo, X. (2019). A new and simple split series strings approach for adding bypass diodes in shingled cells modules to reduce shading loss. *Sol. Energy* 184, 497–507. <https://doi.org/10.1016/j.solener.2019.03.099>.
25. Klasen, N., Weisser, D., Rößler, T., Neuhaus, D.H., and Kraft, A. (2022). Performance of shingled solar modules under partial shading. *Progress in Photovoltaics*. 30, 325–338. <https://doi.org/10.1002/pip.3486>.
26. Klasen, N., Lux, F., Weber, J., Weißer, D., Roessler, T., Kraft, A., and Neuhaus, D.H. (2021). Quantitative evaluation of the shading resilience of PV modules. In 38th European Photovoltaic Solar Energy Conference and Exhibition, pp. 560–567. <https://doi.org/10.4229/EUPVSEC20212021-4BO.2.6>.
27. Carr, A.J., Jansen, M.J., de Bruijne, M., Okel, L., Kloos, M., and Eerenstein, W. (2014). High voltage MWT module with improved shadow performance. In 2014 IEEE 40th Photovoltaic Specialist Conference (PVSC), pp. 2685–2688. <https://doi.org/10.1109/PVSC.2014.6925482>.
28. Slooff, L.H., Carr, A.J., de Groot, K., Jansen, M.J., Okel, L., Jonkman, R., Bakker, J., de Gier, B., and Harthoorn, A. (2017). Shade response of a full size TESSERA module. *Jpn. J. Appl. Phys.* 56, 08MD01. <https://doi.org/10.7567/JJAP.56.08MD01>.
29. Mewe, A.A., Stodolny, M.K., van Roosmalen, J.A., Janssen, G.J., de Keijzer, M.A., Bronsveld, P.C., and Weeber, A.W. (2013). XIS: a low-current, high-voltage back-junction back-contact device. *Energy Proc.* 38, 443–448. <https://doi.org/10.1016/J.EGYPRO.2013.07.302>.
30. Hanifi, H., Pander, M., Jaeckel, B., Schneider, J., Bakhtiari, A., and Maier, W. (2019). A novel electrical approach to protect PV modules under various partial shading situations. *Sol. Energy* 193, 814–819. <https://doi.org/10.1016/j.solener.2019.10.035>.
31. Pannebakker, B.B., de Waal, A.C., and van Sark, W.G. (2017). Photovoltaics in the shade: one bypass diode per solar cell revisited: photovoltaics in the shade. *Prog. Photovolt. Res. Appl.* 25, 836–849. <https://doi.org/10.1002/pip.2898>.
32. Aljafari, B., Satpathy, P.R., and Thanikanti, S.B. (2022). Partial shading mitigation in PV arrays through dragonfly algorithm based dynamic reconfiguration. *Energy* 257, 124795. <https://doi.org/10.1016/j.energy.2022.124795>.
33. Sim, Y.H., Yun, M.J., Lee, D.Y., and Cha, S.I. (2021). Origami-foldable tessellated Crystalline-Si solar cell module with metal textile-based stretchable connections. *Sol. Energy Mater. Sol. Cell.* 231, 111318. <https://doi.org/10.1016/j.solmat.2021.111318>.
34. Yun, M.J., Sim, Y.H., Lee, D.Y., and Cha, S.I. (2022). Reliable Lego®-style assembled stretchable photovoltaic module for 3-dimensional curved surface application. *Appl. Energy* 323, 119559. <https://doi.org/10.1016/j.apenergy.2022.119559>.
35. Sze, S.M. (1981). *Physics of Semiconductor Devices*, second ed (John Wiley and Sons).
36. Markvart, T., and Castañer, L. (2018). Principles of solar cell operation. *McEvoy's Handbook of Photovoltaics: Fundamentals and Applications*, 3–28. <https://doi.org/10.1016/B978-0-12-809921-6.00001-X>.
37. Brum, N. (2022). PyLTSpice. <https://pypi.org/project/PyLTSpice/>.
38. Suckow, S., Pletzer, T., and Kurz, H. (2014). Fast and reliable calculation of the two-diode mode without simplifications. *Prog. Photovoltaics Res. Appl.* 22, 494–501. <https://doi.org/10.1002/pip.2301>.
39. Stephan, S. (2014). 2/3-Diode Fit. <https://nanohub.org/resources/14300>.
40. McKay, M.D., Beckman, R.J., and Conover, W.J. (1979). A comparison of three methods for selecting values of input variables in the analysis of output from a computer code. *Technometrics* 21, 239–245. <https://doi.org/10.2307/1268522>.
41. Deutsch, J.L., and Deutsch, C.V. (2012). Latin hypercube sampling with multidimensional uniformity. *J. Stat. Plann. Inference* 142, 763–772. <https://doi.org/10.1016/J.JSPI.2011.09.016>.
42. Moza, S. (2020). sahil89/lhsmdu: Latin Hypercube Sampling with Multi-Dimensional Uniformity (LHSMU): Speed Boost Minor Compatibility Fixes (1.1.1). Zenodo. <https://doi.org/10.5281/zenodo.3929531>.

## STAR★METHODS

### KEY RESOURCES TABLE

REAGENT or RESOURCE	SOURCE	IDENTIFIER
<b>Chemicals, peptides, and recombinant proteins</b>		
Solaris	Smooth-On	N/A
EpoxAcast 690	Smooth-On	
Oxirane, 2,2'-((1-methylethylidene)bis(4,1-phenyleneoxymethylene))bis-, homopolymer		25085-99-8
Polyoxypropylenediamine		9046-10-0
<b>Software and algorithms</b>		
OriginPro 2019	Origin Lab	<a href="https://originlab.com">https://originlab.com</a>
Python	Python Software Foundation	<a href="https://www.python.org">https://www.python.org</a>
LTspice	Analog Devices	<a href="https://www.analog.com">https://www.analog.com</a>
<b>Other</b>		
MonoX 3D printer	Anycubic	N/A
UV Tough Resin	Anycubic	
(octahydro-4,7-methano-1H-indenediyl)bis(methylene) diacrylate		42594-17-2
Propylidynetrimethanol, ethoxylated, esters with acrylic acid		28961-43-5
diphenyl(2,4,6-trimethylbenzoyl)phosphine oxide		75980-60-8
2-ethyl-2-[[[(1-oxoallyl)oxy]methyl]-1,3-propanediyl] diacrylate		15625-89-5
PERC Solar Cell	Lightway Solar	LWM5BB-PERC-223
Cu Wire	Heesung Material	HSE-02- SR34

### RESOURCE AVAILABILITY

#### Lead contact

Further information and requests for resources, measurement procedures and data can be directed to the lead contact, Dr. Seung I. Cha ([sicha@keri.re.kr](mailto:sicha@keri.re.kr)).

#### Materials availability

All photovoltaics, materials and chemicals could be available commercially.

#### Data and code availability

- All data reported in this paper will be shared by the [lead contact](#) upon request.
- The codes are available on reasonable request from the [lead contact](#).
- Any additional information required to reanalyze the data reported in this paper is available from the [lead contact](#) upon request.

### EXPERIMENTAL MODEL AND SUBJECT DETAILS

We fabricated the conventional module with four cells connected in strings (cell size 60 mm × 60 mm with a square shape), as shown in [Figure 2A](#). In total, this module consisted of four conventional cells. The shingled module was fabricated with four subgroup cells, where each consisting of four cells in strings (cell size 15 mm × 60 mm with a rectangular shape), as shown in [Figure 2A](#). This module consisted of 16 shingled cells. We fabricated the SAHiV module with 12 subgroup cells, where each subgroup cell consisted of four string cells (cell size 15 mm × 20 mm with a rectangular shape), as shown in [Figure 2A](#). This module consisted of 48 SAHiV cells. The SAHiV triangle module was fabricated with 12 subgroup cells, where each subgroup cell consisted of four string cells (cell size 30 mm × 20 mm with the right-triangle shape), as shown in [Figure 2A](#). This module consisted of 48 SAHiV triangle cells.

We used passivated emitter rear cells (LWM5BB-PERC-223, efficiency 22.5%; Lightway Solar, Guangdong, China) with dimensions of  $158.75 \times 158.75 \text{ mm}^2$ ; the cells were cut using a fiber laser. We used silicone encapsulation rubber (Solaris; Smooth-On) as an encapsulant to replace ethylene vinyl acetate (EVA) and glass, which are commonly used in solar cells, to prevent yellowing problems in the cells and improve the solar cell performance. The frame for the cell was fabricated using an Anycubic Photon Mono X 3D Printer with Anycubic UV Tough Resin material and was attached to the cell using EpoxAcast 690.